Supplementary information for

coexistence of quantum anomalous Hall and anomalous Nernst effects in Cr-doped NaMgX (X = P, As, Sb) monolayers

Xianglin Liu, [a] Huiyun Fu, [a] Junjie He, [a] Yuli Xiong, [a] Jie Zhang, [a,*] Shoubing Ding, [a,]

[*] Zhenxiang Cheng, [b,*] and Zhimin Wu [a,*]

[a] School of Physics and Electronic Engineering, Chongqing Normal University, Chongqing 401331, China

[b] Institute for Superconducting and Electronic Materials (ISEM), University of Wollongong, Wollongong 2500, Australia

[*]*Corresponding Authors:*

E-mail: jiezhang@cqnu.edu.cn (J. Zhang),

E-mail: shoubingding@cqnu.edu.cn (S. Ding)

E-mail: cheng@uow.edu.au (Z. Cheng)

E-mail: zmwu@cqnu.edu.cn (Z. Wu)

The NaMgX (X = P, As, Sb) monolayers were constructed by cleaving their bulk counterparts along the (111) crystallographic plane, as shown in Figs. S1(a-b). The calculated positive binding energy (E_b) and negative formation energy (E_f) suggest that these monolayers are likely to form stable bonds and be synthesizable experimentally (Table S1). Furthermore, these structures exhibit robust dynamic and thermodynamic stability, as confirmed by the absence of imaginary frequencies across the full phonon spectra and only minimal energy fluctuations in *ab* initio molecular dynamics (AIMD) simulations at 300 K [Figs. S2(a-b)]. Examination of the band structures of these systems reveals that they exhibit the characteristic of the narrow-bandgap, non-magnetic semiconductor [Fig. S2(c)]. To obtain Cr single- and double-doped NaMgX (X = P, As, Sb) monolayers, we first constructed a 36-atom supercell from the primitive NaMgX (X = P, As, Sb) monolayers [Fig. S1(b)]. A single Cr atom was then introduced by substituting the central Mg atom, resulting in a stable single-doped configuration [Figs. S1(c) and S3(a-b)]. Based on this structure and considering periodicity and symmetry, we identified three potential sites [labeled I, II and III in Fig. S1(d)] for the second Cr atom doping. Figs. 1(c-f), S4 and S5 confirm that all double-doped configurations are dynamically and thermodynamically stable.

The E_b and E_f were computed using the following formulas:

$$E_b = \left(n_{Na}E_{Na} + n_{Mg}E_{Mg} + n_{Cr}E_{Cr} + n_X E_X - E_{Total}\right) \Big/ n_{Na} + n_{Mg} + n_{Cr} + n_X \backslash *$$

MERGEFORMAT (1)

$$E_f = \left(E_{Total} - n_{Na}\mu_{Na} - n_{Mg}\mu_{Mg} - n_{Cr}\mu_{Cr} - n_X\mu_X\right) \Big/ n_{Na} + n_{Mg} + n_{Cr} + n_X \backslash *$$

MERGEFORMAT (2)

Where n_{Na}, n_{Mg}, n_{Cr}, and n_X represent the number of Na, Mg, Cr, and X atoms, respectively. E_{Na}, E_{Mg}, E_{Cr}, E_X represent the energies of an isolated Na, Mg, Cr, and X atoms and E_{Total} is the total energy of the unit cell. Here, the μ_{Na}, μ_{Mg}, μ_{Cr} and μ_X denote the elemental chemical potentials obtained from their stable bulk phases.

The Curie temperature (T_C) was determined using Monte Carlo (MC) simulations implemented in the MCSOLVER package. The calculations were performed on a 16×16×1 supercell. The temperature was scanned from 1 K to 400 K with a total of 51 equally spaced temperature points. To equilibrate the system, the first 40,000 Monte

Carlo steps were discarded as thermalization, followed by 80,000 steps for measuring physical quantities. The Wolff cluster algorithm was adopted for spin updates, and the number of Wolff updates per Monte Carlo step (tau) was set to 15.

Table S1. NaMgX (X = P, As, Sb) monolayers and Their Corresponding Cr-Single-Doped and Cr-Double-Doped Systems: Optimized Lattice Constants, Binding Energies(E_b), Formation Energies(E_f), and Band Gaps(E_g).

2D systems	Lattice (Å)	E_b (eV)	E_f (eV)	E_g (eV)
NaMgP	4.28	2.35	-0.32	1.28
NaMgAs	4.42	2.20	-0.35	0.91
NaMgSb	4.78	1.99	-0.22	1.20
$Na_{12}Mg_{11}CrP_{12}$	14.75	2.33	-0.23	/
$Na_{12}Mg_{11}CrAs_{12}$	15.26	2.17	-0.26	/
$Na_{12}Mg_{11}CrSb_{12}$	16.49	2.00	-0.17	/
$Na_{12}Mg_{10}Cr_2P_{12}$-I	14.68	2.40	-0.24	0.25
$Na_{12}Mg_{10}Cr_2As_{12}$-I	15.23	2.23	-0.25	0.04
$Na_{12}Mg_{10}Cr_2Sb_{12}$-I	16.43	2.02	-0.12	0.21
$Na_{12}Mg_{10}Cr_2P_{12}$-II	14.65	2.39	-0.23	/
$Na_{12}Mg_{10}Cr_2As_{12}$-II	15.18	2.22	-0.25	/
$Na_{12}Mg_{10}Cr_2Sb_{12}$-II	16.41	2.01	-0.11	/
$Na_{12}Mg_{10}Cr_2P_{12}$-III	14.69	2.34	-0.17	/
$Na_{12}Mg_{10}Cr_2As_{12}$-III	15.21	2.18	-0.20	/
$Na_{12}Mg_{10}Cr_2Sb_{12}$-III	16.42	2.01	-0.12	/

Table S2. The energy of non-magnetic(NM), ferromagnetic(FM), and various antiferromagnetic configurations (AFM-1, AFM-2, AFM-3) corresponding to $Na_{12}Mg_{10}Cr_2P_{12}$ monolayer at different U values.

System/U(eV)	1	2	3	4
NM	-228.37	-225.30	-223.03	-221.04
FM	-238.83	-236.93	-235.31	-233.89
AFM-1	-238.73	-236.92	-235.29	-233.87
AFM-2	-238.57	-236.74	-235.23	-233.80
AFM-3	-238.60	-236.84	-235.26	-233.82

Table S3. The energy of non-magnetic(NM), ferromagnetic(FM), and various antiferromagnetic configurations (AFM-1, AFM-2, AFM-3) corresponding to $Na_{12}Mg_{10}Cr_2As_{12}$ monolayer at different U values.

System/U(eV)	1	2	3	4
NM	-212.00	-209.00	-206.85	-205.00
FM	-222.92	-221.12	-219.58	-218.17
AFM-1	-222.57	-220.91	-219.41	-218.04
AFM-2	-222.83	-221.07	-219.52	-218.12
AFM-3	-222.69	-221.00	-219.46	-218.07

Table S4. The energy of non-magnetic(NM), ferromagnetic(FM), and various antiferromagnetic configurations (AFM-1, AFM-2, AFM-3) corresponding to $Na_{12}Mg_{10}Cr_2Sb_{12}$ monolayer at different U values.

System/U(eV)	1	2	3	4
NM	-193.07	-189.76	-186.71	-183.88
FM	-204.35	-202.60	-201.02	-199.54
AFM-1	-204.28	-202.54	-200.97	-199.50
AFM-2	-203.96	-202.28	-200.64	-199.20
AFM-3	-204.13	-202.39	-200.85	-199.44

Table S5. Magnetic exchange coupling constants J_2, J_3 and single-ion anisotropy parameters of the $Na_{12}Mg_{10}Cr_2X_{12}$ (X = P, As, Sb) monolayers.

2D systems	J_2 (meV)	J_3 (meV)	A (μeV)
$Na_{12}Mg_{10}Cr_2P_{12}$	-0.16	-0.04	28.59
$Na_{12}Mg_{10}Cr_2As_{12}$	-0.17	-0.08	-10.39
$Na_{12}Mg_{10}Cr_2Sb_{12}$	-0.10	-0.03	-80.23

Table S6. Here are the Curie temperatures (T_C), SOC-induced band gaps, and anomalous Nernst effect (ANE) coefficients of some classic two-dimensional (2D) ferromagnetic materials.

2D systems	T_C (K)	Band gap (meV)	ANE coefficient [A/(m·K)]	Ref
CrI_3	45	/	/	43
$Cr_2Ge_2Te_6$	20	/	/	44
Zn_2N_3	168	4.3	/	47
$NiAsO_3$	216.3	4.2	/	48
$NiBiO_3$	258	1.5	/	49
CrP	500	/	0.003	57
$FePd_2Te_2$	183	/	0.15	58
Fe_3GeTe_2	150	/	0.28	59

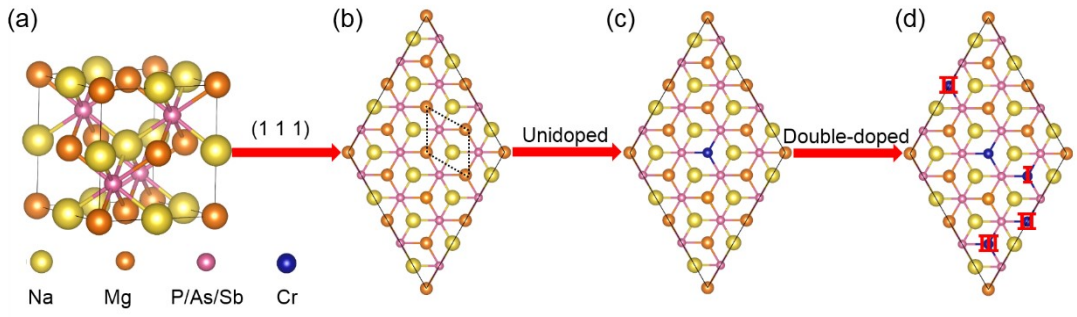

Fig. S1. (a) 3D NaMgX (X=P, As, Sb). (b) NaMgX (X=P, As, Sb) monolayers, the black dashed line represents the primitive cell. (c) Cr single doped NaMgX (X=P, As, Sb) monolayers. (d) Cr double doped NaMgX (X=P, As, Sb) monolayers, the red I, II and III represent possible sites for substitution doping of the second Cr atom.

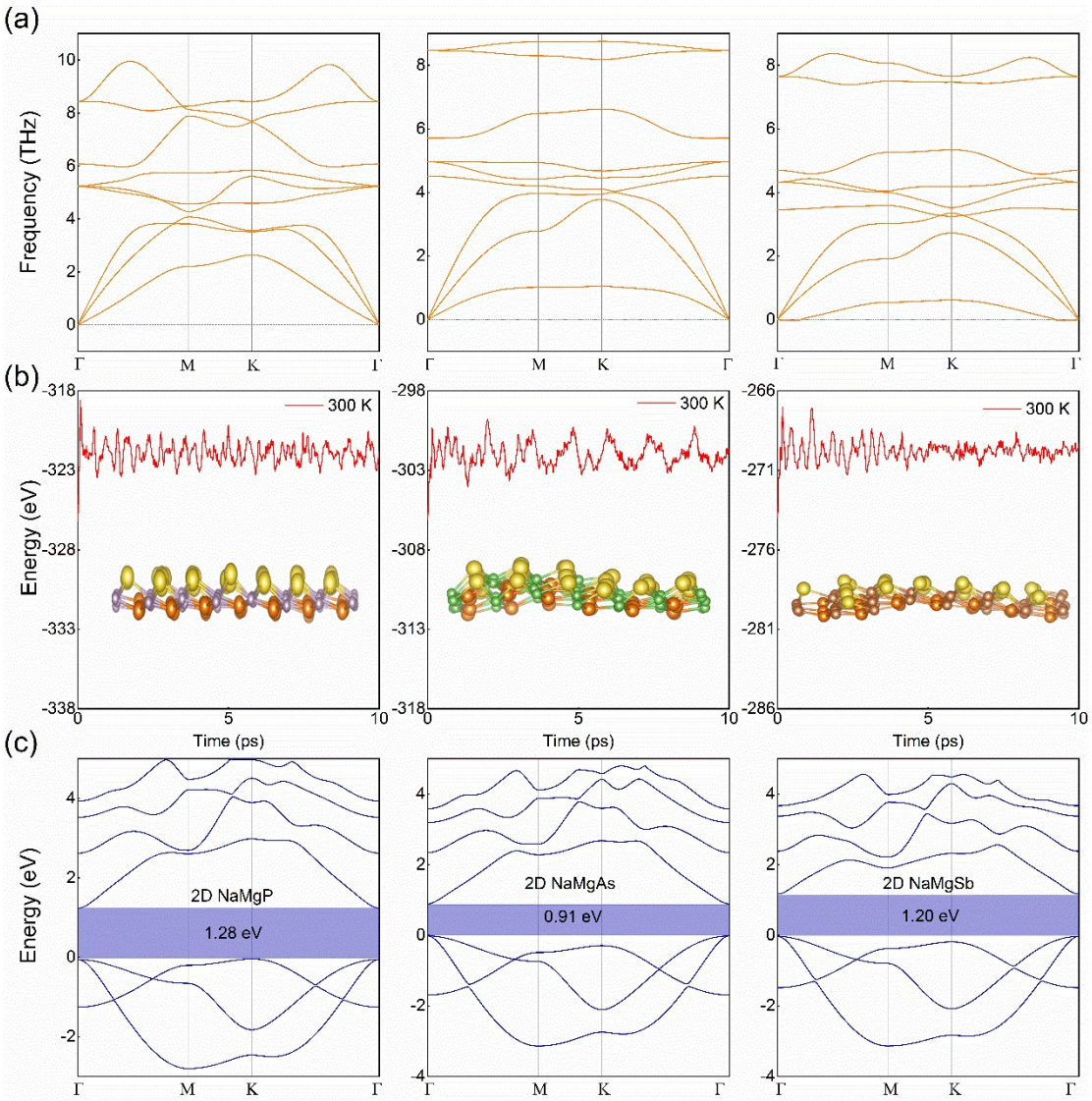

Fig. S2. NaMgX (X=P, As, Sb) monolayers: (a) Phonon spectra. (b) AIMD simulations. (c) Band structures.

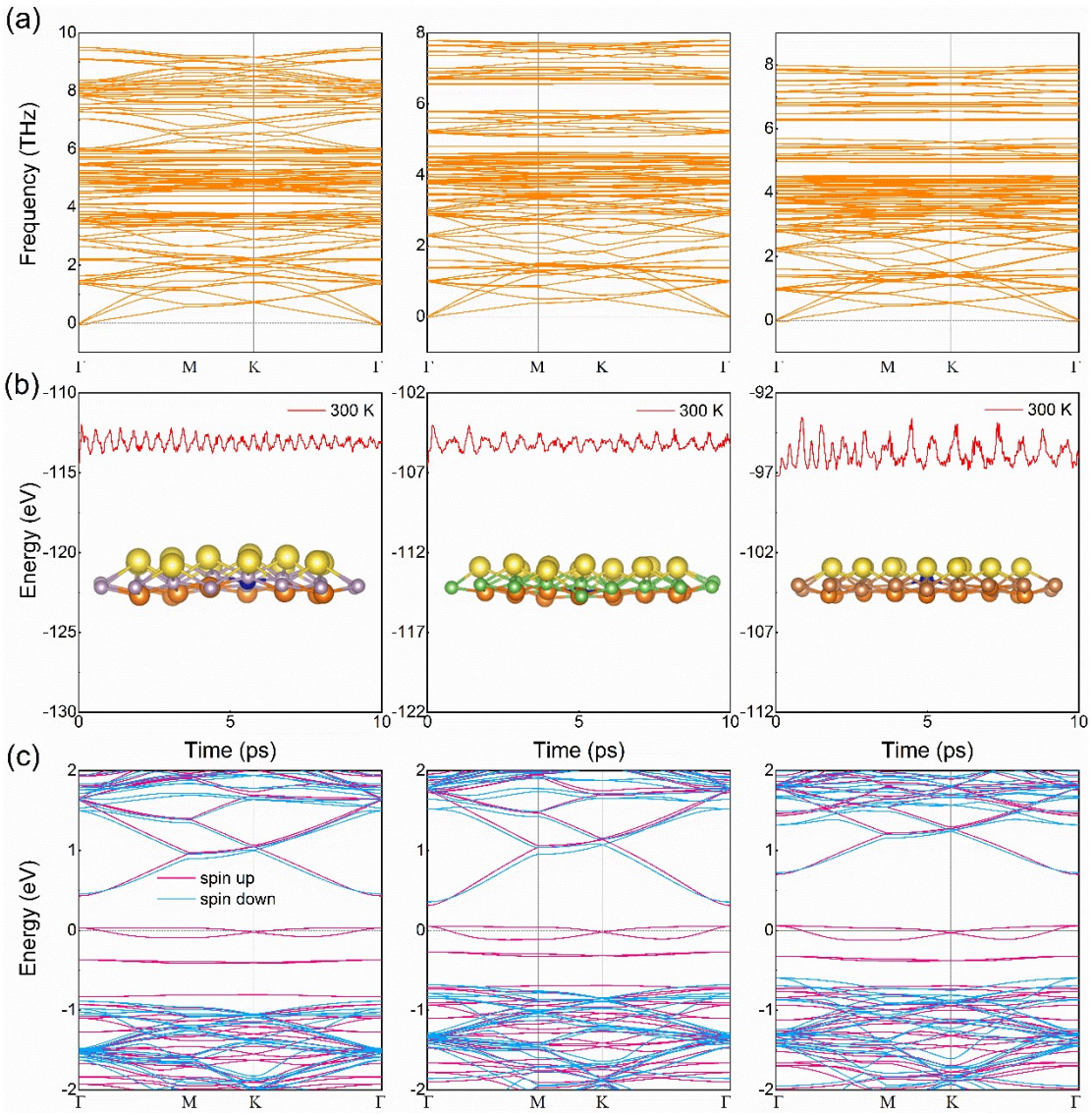

Fig. S3. Cr single-doped NaMgX (X=P, As, Sb) monolayers: (a) Phonon spectra. (b) AIMD simulations. (c) Band structures.

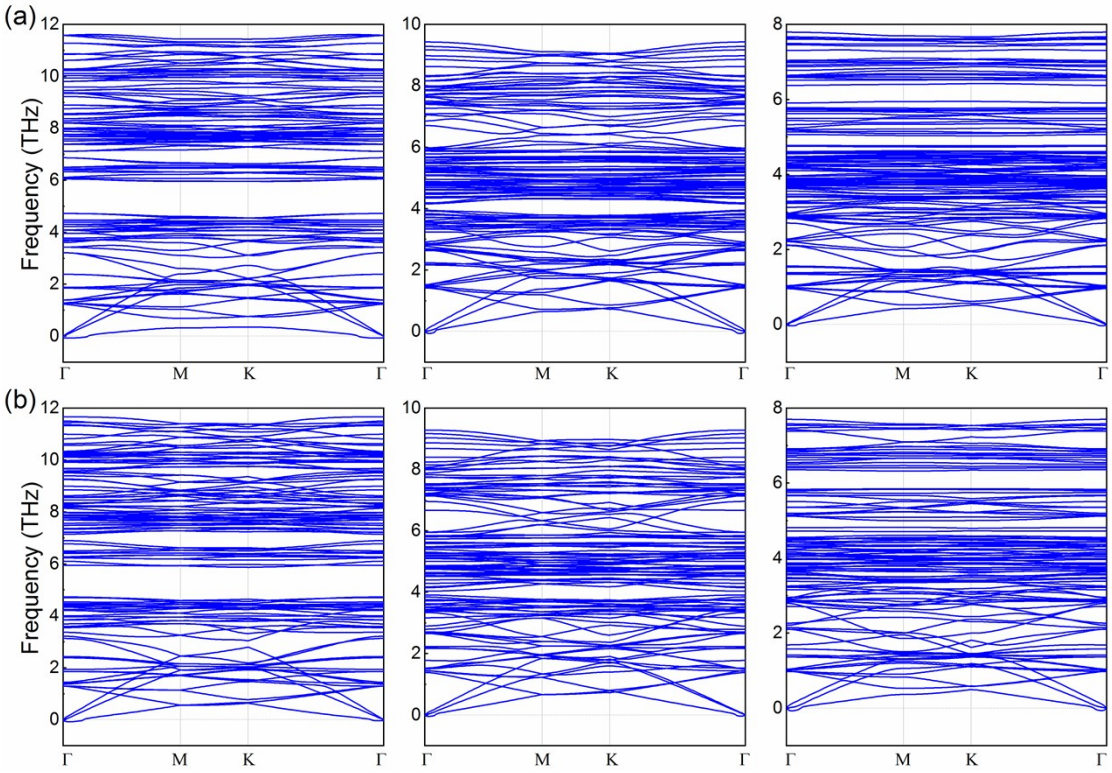

Fig. S4. Phonon spectra of Cr double-doped doped NaMgX (X = P, As, Sb) monolayers: (a) Configuration I. (b) Configuration II.

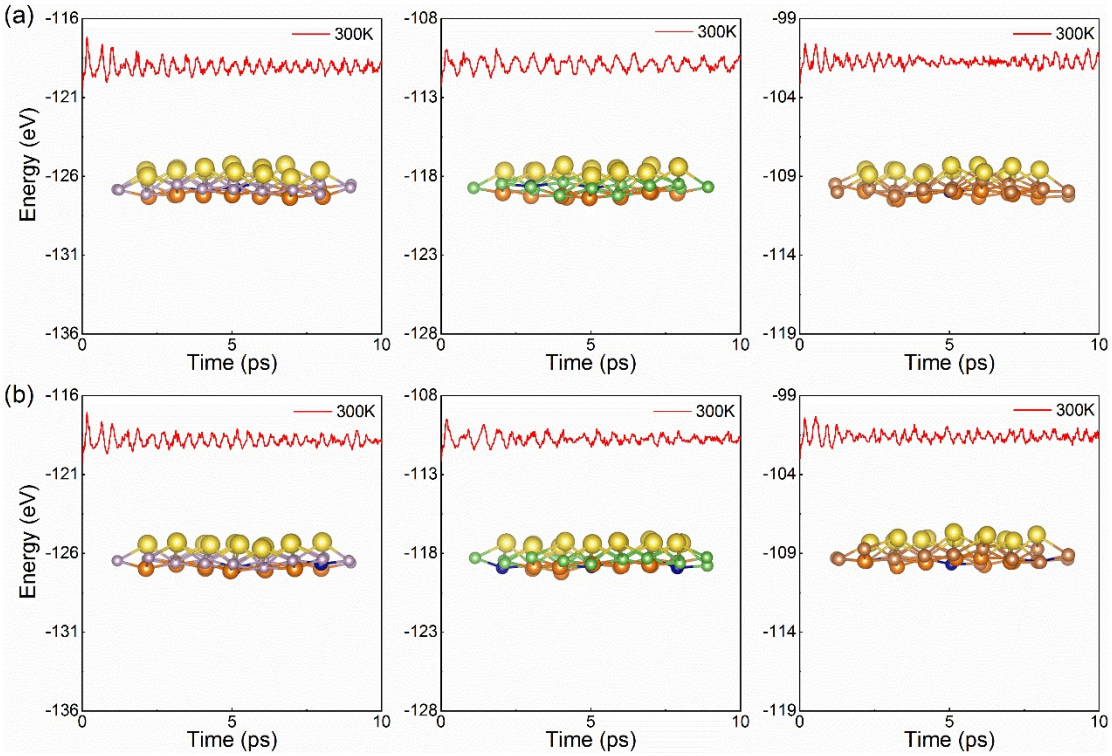

FIG. S5. AIMD simulations of Cr double-doped NaMgX (X = P, As, Sb) monolayers: (a) Configuration I. (b) Configuration II.

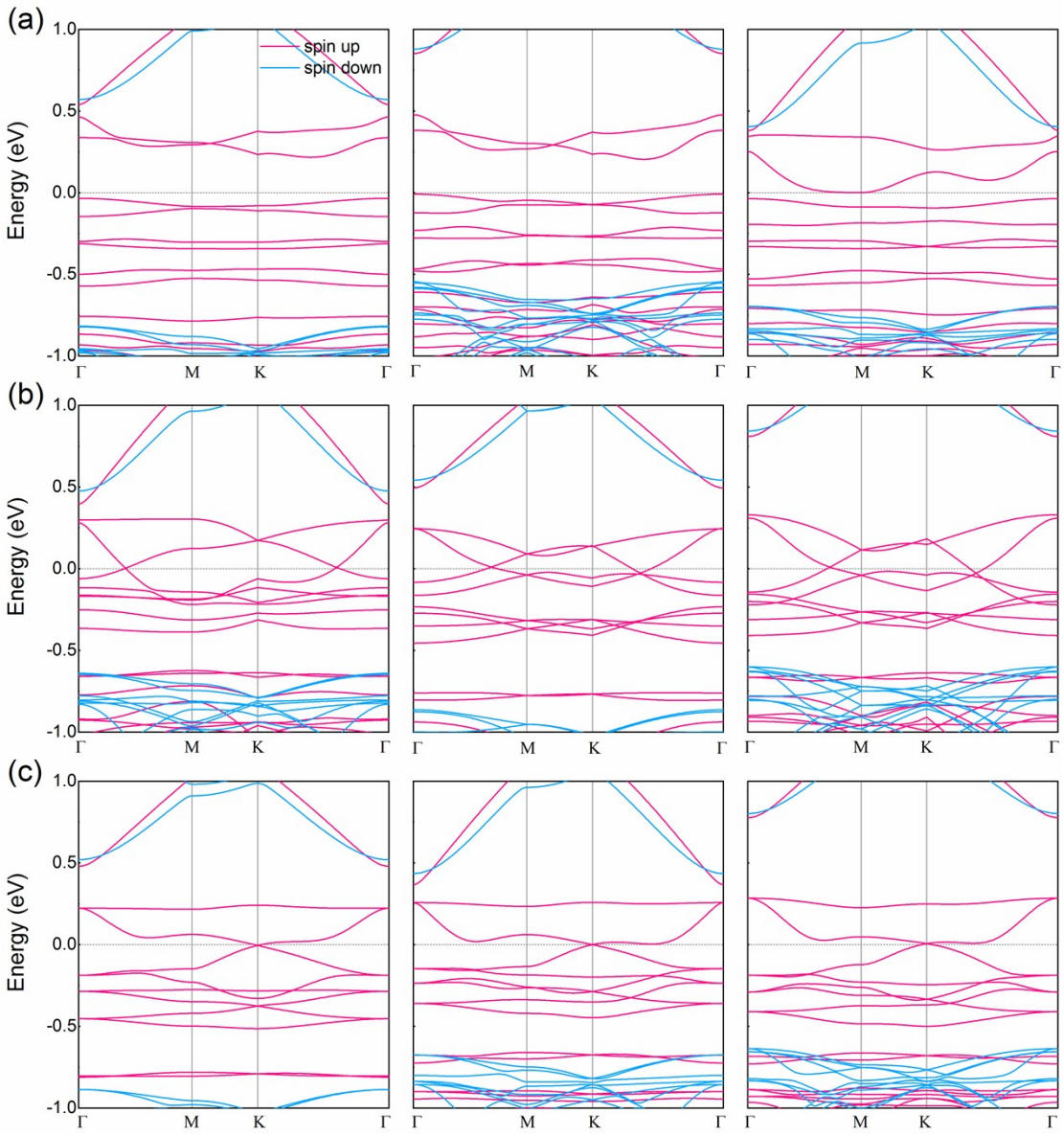

Fig. S6. The band structures corresponding to the Cr-double doped NaMgX (X=P, As, Sb) monolayers: (a) Configuration I. (b) Configuration site. (c) Configuration III site.

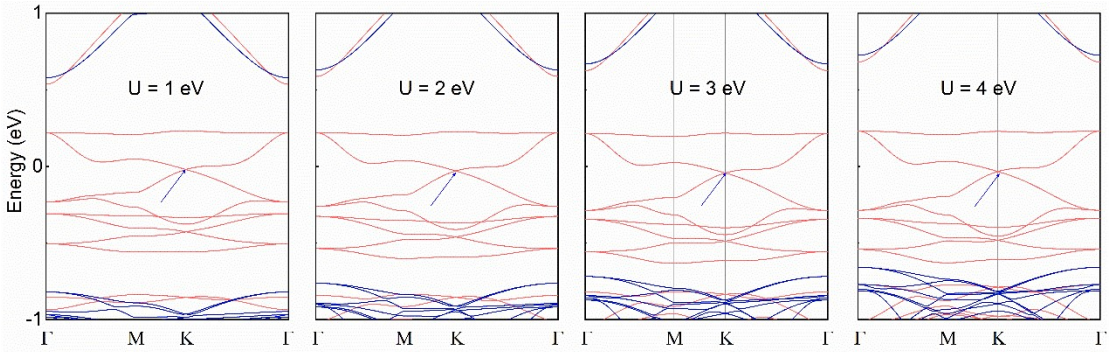

Fig. S7. The band structures of $Na_{12}Mg_{10}Cr_2P_{12}$ monolayer corresponding to different U values (1–4 eV).

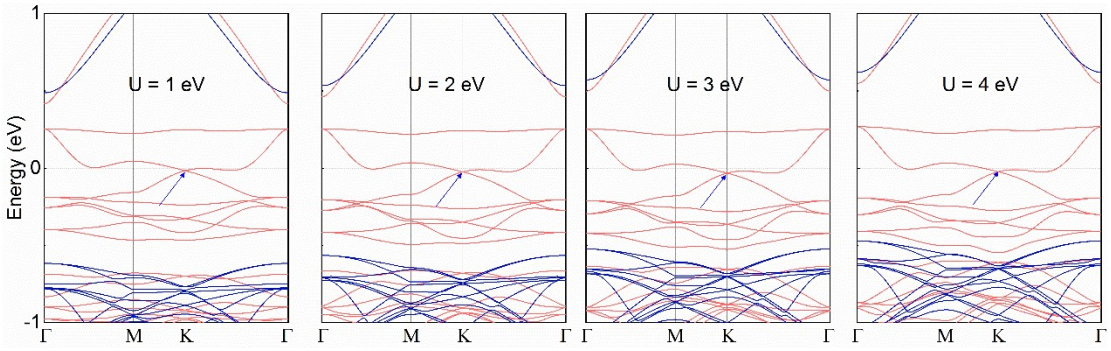

Fig. S8. The band structures of $Na_{12}Mg_{10}Cr_2As_{12}$ monolayer corresponding to different U values (1– 4 eV).

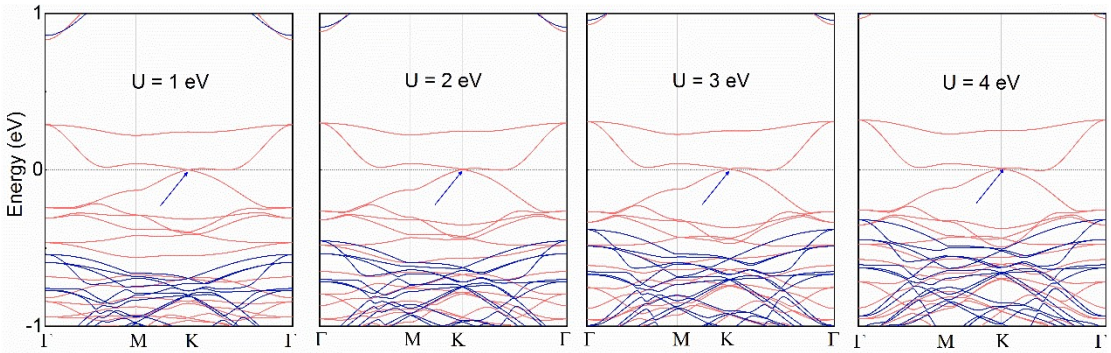

Fig. S9. The band structures of $Na_{12}Mg_{10}Cr_2Sb_{12}$ monolayer corresponding to different U values (1– 4 eV).

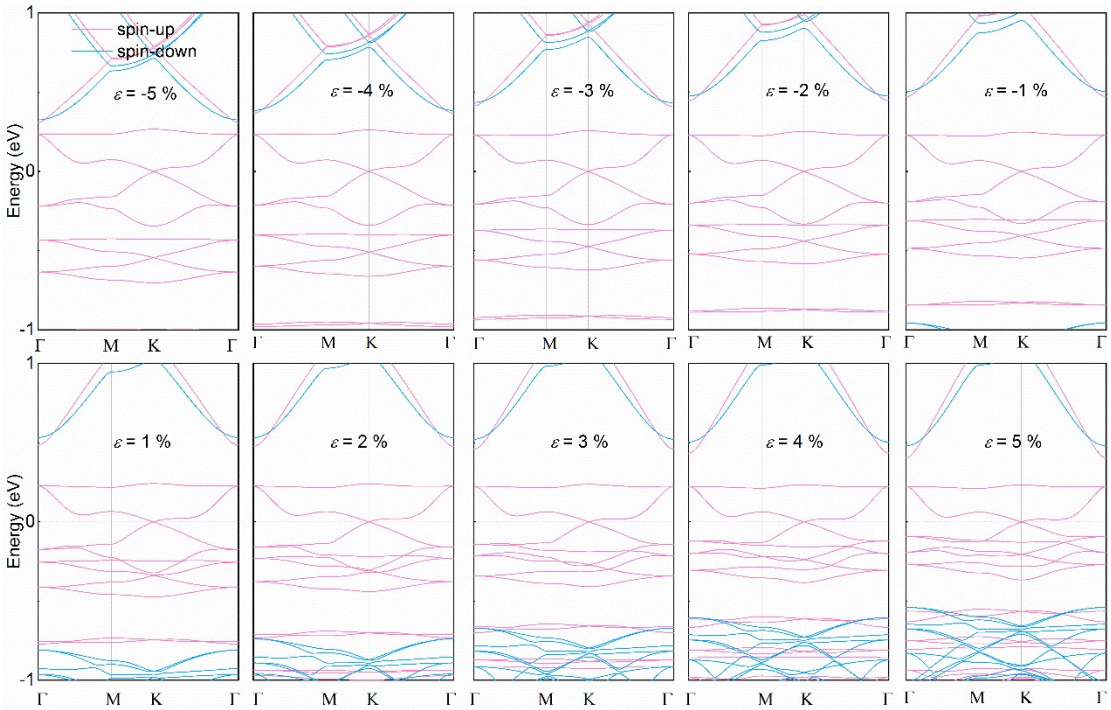

Fig. S10. Band structures of the $Na_{12}Mg_{10}Cr_2P_{12}$ monolayer under various biaxial strains (-5%~5%).

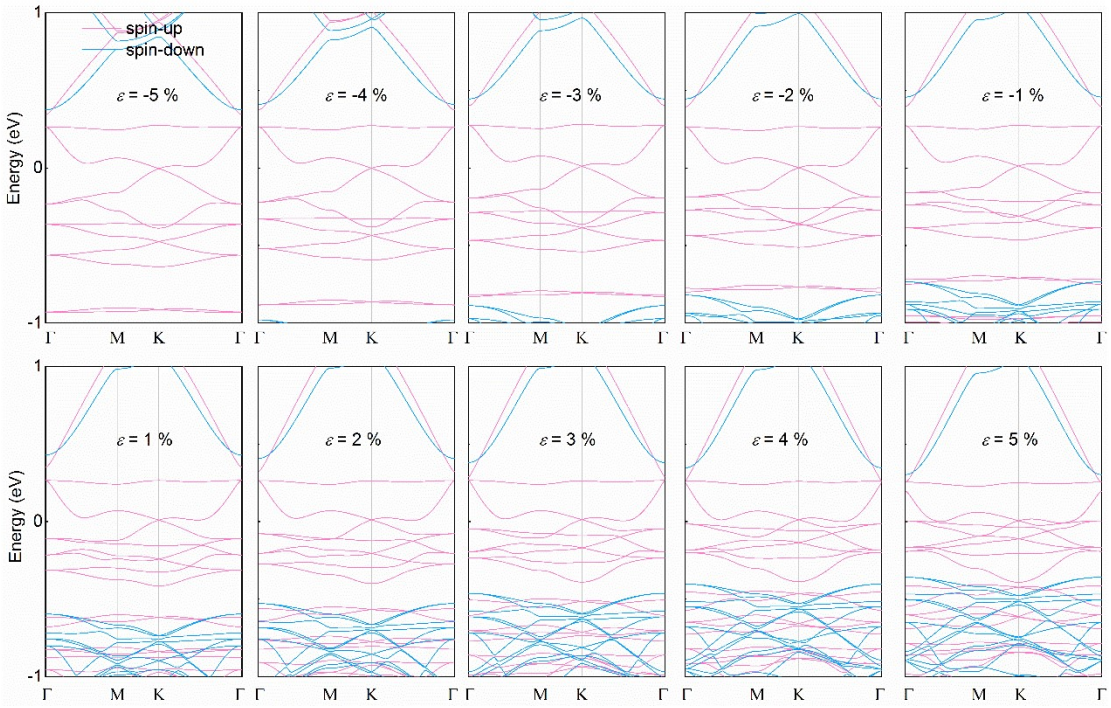

Fig. S11. Band structures of the $Na_{12}Mg_{10}Cr_2As_{12}$ monolayer under various biaxial strains (-5%~5%).

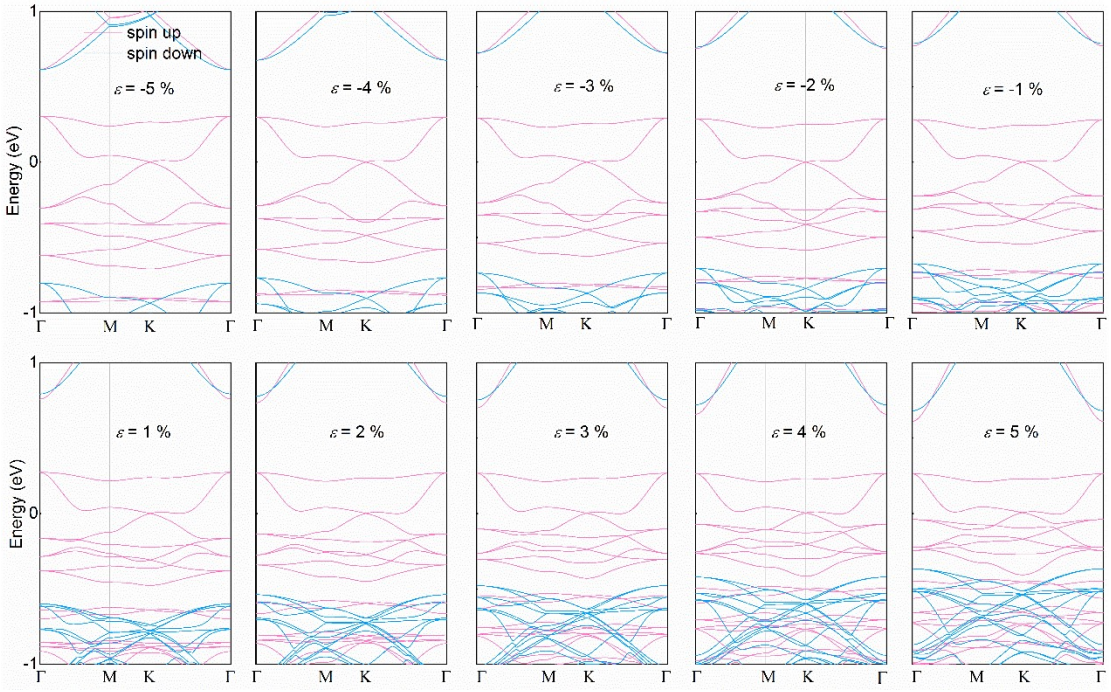

Fig. S12. Band structures of the $Na_{12}Mg_{10}Cr_2Sb_{12}$ monolayer under various biaxial strains (-5%~5%).

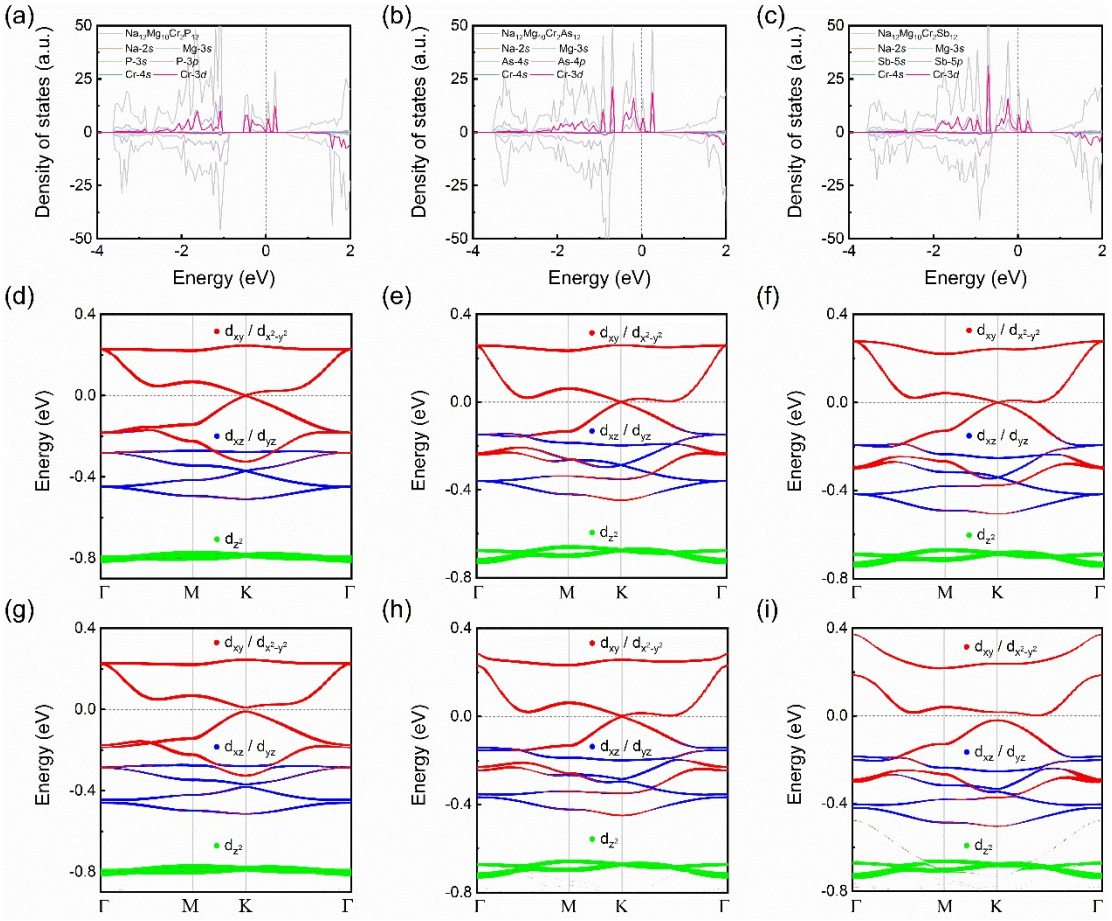

Fig. S13. (a-c) The total density of states (DOS) and projected DOS. (d-f) Cr-3*d* orbital-projected band structures without SOC. (g-i) Cr-3*d* orbital-projected band structures with SOC.

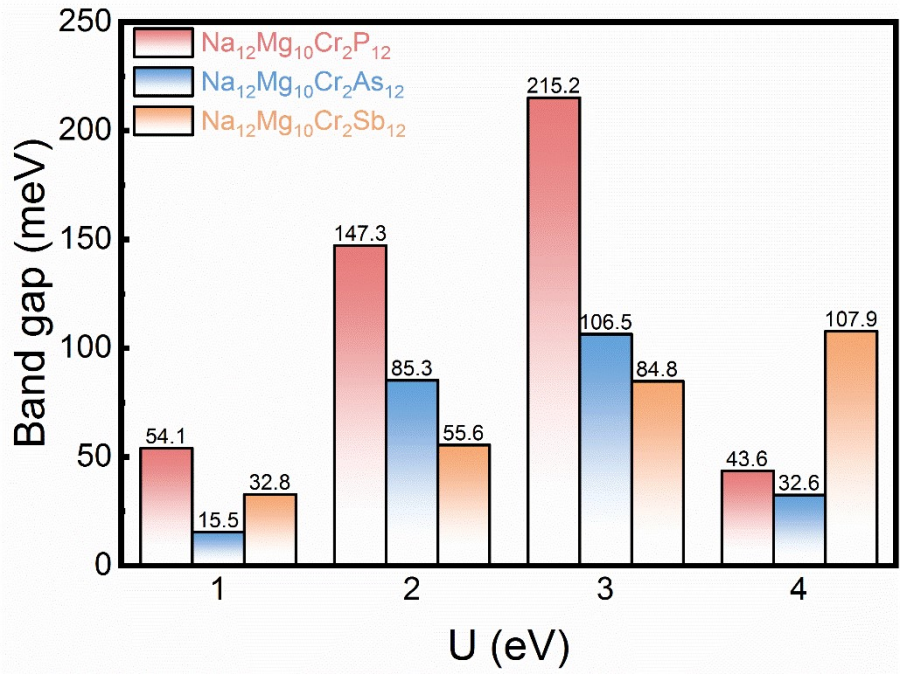

Fig. S14. When considering SOC, the corresponding band gap of the $Na_{12}Mg_{10}Cr_2X_{12}$ (X = P, As, Sb) monolayers under different U values (U = 1,2,3,4 eV).